Mobile small polarons and the Peierls transition in the quasi-one-dimensional conductor $K_{0.3}MoO_3$

L. Perfetti, S. Mitrovic, G. Margaritondo, and M. Grioni
Institut de Physique des Nanostructures, EPF Lausanne, CH-1015 Lausanne, Switzerland

L. Forró
Institu de Physique de la Matière Complexe, EPF Lausanne, CH-1015 Lausanne, Switzerland

L. Degiorgi
Laboratorium für Festkörperphysik, ETH Zurich, CH-8093 Zurich, Switzerland

H. Höchst
Synchrotron Radiation Center, University of Wisconsin, Stoughton, Wisconsin 53589-3097
(Received 9 April 2002; published 5 August 2002)

High-resolution angle-resolved photoemission spectroscopy (ARPES) on the quasi-one-dimensional Peierls system $K_{0.3}MoO_3$ reveals a ''hidden'' open Fermi surface and band features displaying the symmetry properties of the underlying lattice. However, the ARPES line shapes and optical data suggest that the corresponding quasiparticles are heavily renormalized by strong electron-phonon interactions. The temperature dependence of the leading edge of the mostly incoherent spectrum bears signatures of the Peierls transition at $T_P=180$ K and of pretransitional fluctuations.

DOI: 10.1103/PhysRevB.66.075107 PACS number(s): 71.45.Lr, 71.10.Pm, 71.38.Cn, 79.60.−i

I. INTRODUCTION

Lattice periodicity and band filling determine the behavior of charge carriers, and ultimately the electronic properties of solids, in the limit of vanishing interactions. This is no longer true in strongly interacting systems, where translational symmetry is not necessarily manifest in the wave functions of individual carriers. The renormalized single-particle excitations—or quasiparticles (QP's)—postulated by Fermi liquid theory, can be quite different from the bare electrons, and new phases with distinct macroscopic properties may appear.

Quasi-one-dimensional (1D) materials exhibit typical electronic instabilities, like the much studied metal-insulator Peierls transition to a charge-density-wave (CDW) state. Understanding how the QP's evolve into the ordered phase, where the one-to-one correspondence with the noninteracting particles is lost, is of fundamental interest. The accepted picture of the CDW instability emphasizes extended, periodic states and the topology of the 1D Fermi surface, which is perfectly ''nested'' on itself by a translation with wave vector $Q_{CDW}=2k_F$ (k_F is the Fermi wave vector).[1] This weak-coupling theory describes quite successfully the superstructures revealed by scattering experiments, but elements of the opposite strong-coupling scenario[2] may be relevant in materials where the charge density modulations are large.

One-dimensional materials are also of current interest for their *normal* phase. Strictly 1D metallic systems are not Fermi liquids, but Luttinger liquids,[3] with peculiar properties like spin-charge separation and correlation functions characterized by nonuniversal exponents.[4] 1D systems with gaps in the spin sector—especially relevant for the Peierls instability—or in the charge sector are also possible. They are neither Fermi nor Luttinger liquids, but belong to the Luther-Emery of Mott-insulator universality classes.[5,6] Recent spectroscopic work, namely, by optics[7] and photoemission,[8] aimed at identifying the unique spectral features of these correlated 1D states. Signatures of spin-charge separation have been reported in 1D Mott insulators,[9] while data on conductors, either inorganic like $Li_{0.9}Mo_6O_{17}$ (Ref. 10) or organic like TTF-TCNQ (Ref. 11), and on artificial 1D surface nanostructures[12] are still debated. Puzzling, common aspects of the angle-resolved photoemission spectroscopy (ARPES) spectra are the broad line shapes and deep pseudogap features.

Strong pretransitional fluctuations in a broad temperature range between the real (T_P) and the expected mean-field (T_{MF}) transition temperatures are another typical feature of the physics of 1D Peierls materials. Fluctuations are manifest in the temperature dependence of the CDW correlation length extracted from diffraction data.[13] They also influence the electronic states, causing the opening of a pseudogap at the Fermi level.[14–16] The spin susceptibility,[17] specific heat, and optical conductivity[18] of 1D Peierls systems bear signatures of the pseudogap. CDW-related superstructures are also observed above T_P by ARPES.[19,20]

In this paper we address the nature of the QP states and the spectral signatures of the CDW in a typical 1D Peierls material: the Mo blue bronze $K_{0.3}MoO_3$. We find valence states with the symmetry properties predicted by band structure calculations, including a good Fermi surface (FS) nesting at the CDW wave vector. We also find that the energy of these dispersing features is not related to the low-energy properties of the material. By analogy with our recent study of $(TaSe_4)_2I$, another typical Peierls material,[21] we interpret the peculiar line shape as the result of strong interactions with the lattice, leading to the formation of small polarons with strongly renormalized masses. This hypothesis is supported by a new analysis of the optical data. From temperature-dependent momentum distribution curves mea-

sured at the Fermi surface we identify, within a polaronic scenario, the spectral signatures of the Peierls transition and of pretransitional fluctuations. These results suggest that elements of both the weak- and strong-coupling theories should be included in a description of the metal-insulator transition.

II. EXPERIMENT

Single crystals of $K_{0.3}MoO_3$, of typical size $3\times1.5\times0.5$ mm^3, presented a strongly anisotropic electrical resistivity and semiconducting behavior below $T_P=180$ K, in agreement with the literature.[22] We performed ARPES measurements at the PGM beamline and NIM4 beamlines of the Wisconsin Synchrotron Radiation Center (SRC). Photoelectron intensity maps were acquired with a Scienta SES-200 analyzer, with energy and momentum resolution $\Delta E=15$ meV and $\Delta k=0.015$ Å^{-1}, respectively. The samples, mounted at the tip of a closed-cycle He refrigerator, were post-cleaved at $T=60$ K at a pressure of 6×10^{-11} mbar, to expose mirrorlike $(\bar{2}01)$ surfaces. Special care was taken to minimize radiation exposure, and we did not observe noticeable signs of surface degradation over a period of several hours.

The discussion of the optical properties is based on the original data of Ref. 18, obtained over an extended frequency range ($0.1–10^5$ cm^{-1}) as a function of temperature and employing a wealth of methods such as optical reflectivity and resonant cavity techniques. The optical conductivity was determined from the complete absorptivity spectrum by a Kramers-Kronig analysis, as described in Ref. 18.

III. STRUCTURAL AND ELECTRONIC PROPERTIES

$K_{0.3}MoO_3$ has a side-centered monoclinic structure, where double chains built from MoO_6 octahedra run along the crystallographic **b** direction, supporting Mo $4d$–O $2p$ hybrid bands with strong 1D character. The interaction between adjacent double chains splits these bands into bonding (B) and antibonding (AB) subbands which are doped by charge transfer from the K^+ ions.[23,24] These bands generate two pairs of open Fermi surface sheets, perpendicular to the ΓY direction (**b**), with distinct Fermi wave vectors k_F^B and k_F^{AB}. Due to interchain coupling, the FS's are slightly warped, with alternate concavities. Tight-binding calculations[23] and measurements of the transverse CDW correlation length[25] yield a transverse dispersion $4t_\perp\sim0.1$ eV, where $t_\perp$ is the in-plane hopping matrix element. A more recent *ab initio* band structure calculation, performed with the generalized gradient approximation (GGA) scheme, finds nearly flat FS sheets.[26]

The metallic state is unstable below $T_P=180$ K. The CDW formation has been associated with the alternate nesting of the B and AB FS sheets with a single wave vector $Q_{CDW}=(0,q_b,1/2)$, where $q_b=(k_F^B+k_F^{AB})$ is incommensurate ($q_b=0.73b^*;b^*=2\pi/b$) at T_P and locks in to the commensurate value $q_b=0.75b^*$ below 100 K.[22] The saturation value of the Peierls gap is $2\Delta_0=100–150$ meV, from optics and resistivity,[18] consistent with ARPES.[27,28]

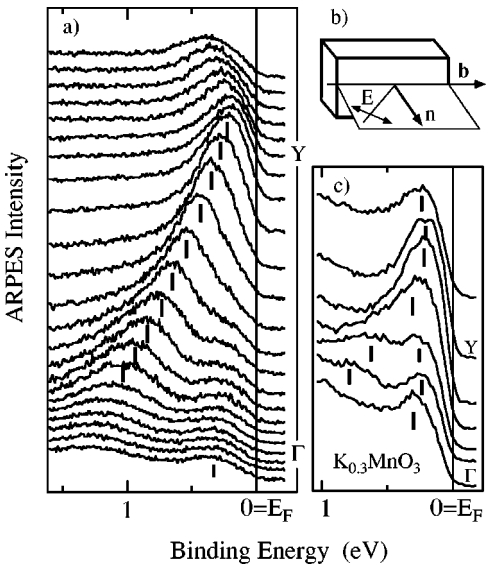

FIG. 1. (a) ARPES spectra acquired along the **b** (ΓY) direction ($T=210$ K, $h\nu=21$ eV). (b) Setup of the ARPES experiment. Notice that the polarization plane is perpendicular to the surface and contains the direction of the chains. (c) Spectra measured with unpolarized light (from Ref. 31).

IV. RESULTS AND DISCUSSION

A. Symmetry of the bands and the Fermi surface

Figure 1(a) shows ARPES spectra measured in the metallic phase ($T=210$ K) along the 1D chain direction **b** (ΓY). Photoelectrons excited by linearly π-polarized light were collected in the (horizontal) plane containing the surface normal, the **b** direction, and the photon beam [Fig. 1(b)]. This geometry selects initial states that are even under a reflection from this plane. A prominent spectral feature disperse from ~1.2 eV at Γ, the center of the Brillouin zone (BZ), to a minimum binding energy of 0.2 eV near the zone boundary $Y=(\pi/b)=0.415$ Å^{-1}. A second, much weaker feature is observed around Γ at smaller binding energy. They represent the B (at higher binding energy) and AB (closer to E_F) subbands. Their dispersion is well described by the more recent band structure calculation.[26] The spectra are consistent with published ARPES data,[28–30] but there is a remarkable difference with respect to data measured with unpolarized radiation [Fig. 1(c), from Ref. 31], where the AB and B structures have comparable intensities.

The large polarization dependence suggests that the two bands have different symmetries. This is supported by scans above and below the horizontal plane. The acceptance window of the analyzer allowed us to collect photoelectrons within $\pm6°$ of the plane, or 65% of the BZ in the ΓX direction, perpendicular to the chains. The results are summarized in the intensity maps of Fig. 2, for various values of the in-chain wave vector $k_\parallel$. The B and AB bands, both well visible at $0.38\Gamma Y$, move towards the Fermi level as $k_\parallel$ increases, and the AB band disappears altogether as the zone boundary is approached.

The perpendicular dispersion is very small (<0.1 eV) and consistent with an open Fermi surface. On the horizontal

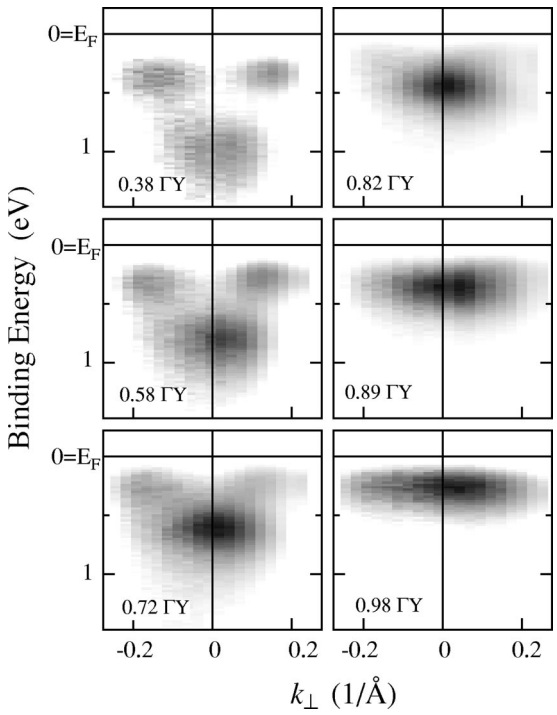

FIG. 2. ARPES intensity maps measured perpendicular to the chains, for various values of the wave vector along the chains $k_{\|}$ ($T=180$ K, $h\nu=21$ eV). Darker regions correspond to larger intensity.

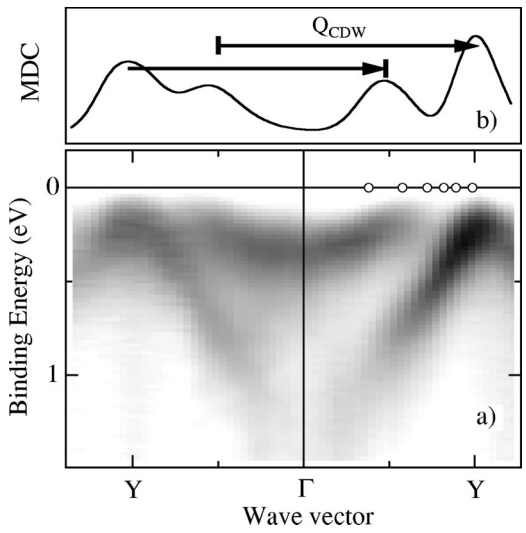

FIG. 3. (a) ARPES intensity map showing the band structure along ΓY ($T=180$ K, $h\nu=21$ eV). The open symbols mark the k locations corresponding to the maps of Fig. 2. (b) Momentum distribution curve (MDC) extracted from (a) at $E=30$ meV ($\Delta E=60$ meV), showing the alternate nesting of the FS sheets.

plane ($k_{\perp}=0$) and for all values of $k_{\|}$, the intensity of band B is maximum and that of band AB is zero. Therefore the two bands have opposite reflection symmetries: *even* for B and *odd* for AB. These are, in the 2D limit, the symmetry properties of the bonding and antibonding combinations of 1D orbitals, discussed in Ref. 24. Opposite reflection symmetries of the nested FS sheets are also consistent with the observed out-of-phase modulation of the lattice positions in adjacent chains.[25,32]

In order to map both bands along the **b** direction, we integrated the photoelectron signal over the full perpendicular angular window of the analyzer, taking advantage of the negligible perpendicular dispersion [Fig. 3(a)]. The B band does not differ from data collected with a narrow perpendicular angular acceptance in the horizontal plane, but in that case the dispersion of band AB could only be monitored when the **b** axis was not exactly horizontal. A remarkable aspect of the data is the absence of a well-defined Fermi surface in the metallic phase. The closest approach to the Fermi level is near $\pi/2b$ (AB) and $Y=\pi/b$ (B), and both bands have ''shadow'' replicas beyond those points. The replica of the AB band is well visible in the perpendicular cuts (at $0.58\Gamma Y$ and $0.72\Gamma Y$) of Fig. 2. Strong shadow bands were also observed in the 1D Peierls system $(TaSe_4)_2I$,[19] but not as clearly, due to the smaller energy separation between analogous bonding and antibonding conduction bands in that compound.

In the Peierls scenario of the CDW formation in $K_{0.3}MoO_3$, the momentum separation between the nested AB and B Fermi surface sheets determines the CDW wave vector.[23] It is not possible to determine Fermi level crossing points from Fig. 3(a). We used instead momentum distribution curves (MDC's), i.e., momentum-dependent constant-energy cuts. The MDC extracted immediately below E_F [Fig. 3(b)] shows four distinct peaks connected in pairs, within experimental accuracy, by $Q_{CDW}=0.75\pi/b$, consistent with scattering data. Similar values of Q_{CDW} have been reported,[28,30] but the individual Fermi wave vectors $k_F^{AB}=0.61\pi/b$, $k_F^B=0.86\pi/b$ (Ref. 30) or $k_F^{AB}=0.59\pi/b$, $k_F^B=0.89\pi/b$ (Ref. 28) are somewhat different. The origin of these differences is not clear. The symmetric intensity distribution (Fig. 2) and dispersion [Fig. 3(a)] rule out spurious effects and give us some confidence in the accuracy of our data.

MDC's measured at various binding energies near the zone boundary (Fig. 4) show a main peak for $k<\pi/b$ and a weaker one at an approximately symmetric location in the second zone, from the ''shadow'' band. Approaching E_F the two features converge towards $k=0.4$ Å^{-1} or $0.96\pi/b$. A detailed analysis of these curves is difficult due to the varying intensities and the interfering effects of umklapps from the lattice and CDW potentials acting, respectively, at $k=\pi/b=0.415$ Å^{-1} and at $k_F^B=0.4$ Å^{-1}. The existence of a shadow replica of the AB band around k_F^{AB}, clearly unrelated to the lattice periodicity, demonstrates that scattering on the CDW potential is certainly important.

B. Peierls transition

In a mean-field theory, the CDW transition removes the entire Fermi surface—or leaves at most small pockets due to imperfect nesting in 2D or 3D—below T_P. This simple description does not apply to the blue bronze. In the metallic phase the dispersing spectral features remain well below the Fermi surface, forming a ''pseudogap,'' which is broader

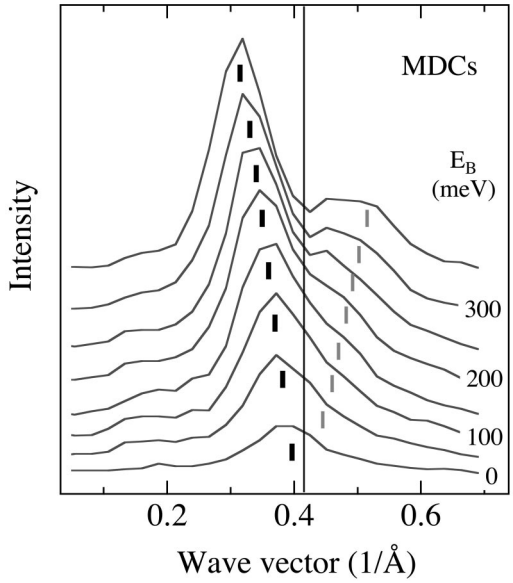

FIG. 4. MDC's extracted at different binding energies ($\Delta E = 30$ meV) near the Y zone boundary. The dashed lines are guides to the eye ($T = 180$, $h\nu = 21$ eV).

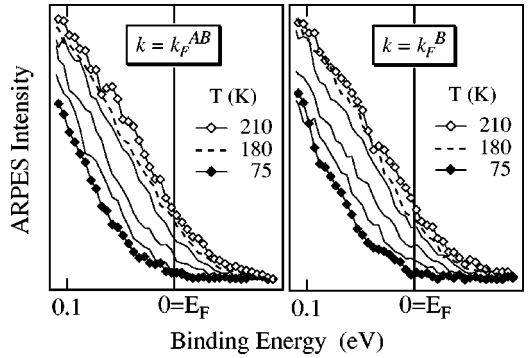

FIG. 6. Temperature evolution of the leading edge of spectra measured at k_F^B and at k_F^{AB} between $T = 210$ K and $T = 75$ K.

than the optical pseudogap[18] and whose origin needs to be clarified. A careful analysis reveals a temperature dependence associated with the Peierls transition at the high-energy end of the spectra. This is illustrated in Figs. 5(a) and 5(b) by ARPES maps collected at 210 K and 75 K, near the maximum of the B band. At 210 K, while the main band feature is at finite binding energy, a very small but finite intensity "spills over" beyond E_F. The MDC measured at the Fermi level at T_P [Fig. 5(c)] exhibits a Lorentzian line shape, the typical fingerprint of a QP. By analogy with $(TaSe_4)_2I$,[21] we take this as spectroscopic evidence of a "hidden" Fermi surface.

The Peierls transition affects both conduction bands, as shown by spectra measured near E_F at both Fermi wave vectors (Fig. 6). Below T_P the leading edges of both bands progressively shift to higher binding energies, until a true gap is formed. The temperature evolution of the two bands is consistent with Ref. 28 and substantiates the accepted scenario requiring that both pairs of FS sheets be involved in the formation of the CDW state. It would be difficult to obtain from Fig. 6 a quantitative description of the changes occurring through the CDW transition, without making specific assumptions on the line shape. Following our analysis of the Peierls transition in $(TaSe_4)_2I$,[21] we used instead MDCs measured across the transition. The starting point is the MDC measured at E_F and T_P, which exhibits a Lorentzian line shape. Below T_P both the intensity and line shape of the MDC are preserved if the cut is performed [Fig. 5(c)] at a higher binding energy $\Delta(T)$. Figure 7(a) shows that $\Delta(T)$ behaves as a phenomenological order parameter for the transition and saturates below $T \sim 100$ K to $\Delta_0 = 60$ meV, consistent the Peierls (half-)gap value from transport and optics.[18]

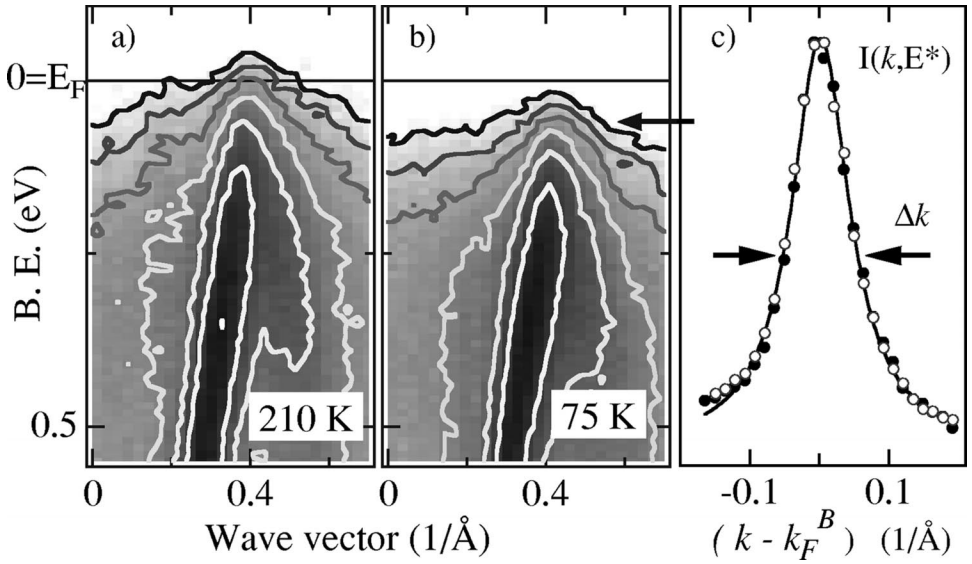

FIG. 5. ARPES intensity maps along ΓY at $T = 210$ K (a) and $T = 75$ K (b). A logarithmic intensity scale was chosen to enhance the small signal near the Fermi level. Lines of constant intensity are indicated. (c) MDC's extracted at the Fermi level at $T = 180$ K (solid circles) and at $E = 60$ meV [arrow in (b)] at $T = 60$ K (open symbols). The solid line is a Lorentzian fit [full width at half maximum (FWHM) $= 0.1$ Å^{-1}].

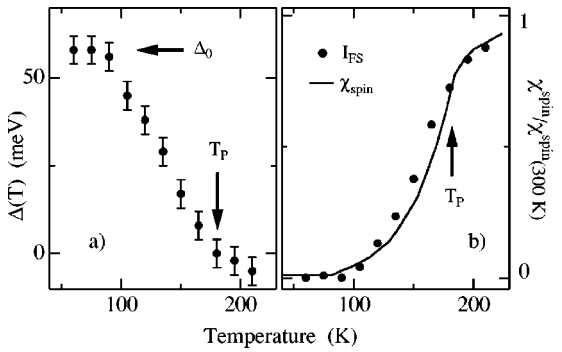

FIG. 7. (a) Single-particle gap extracted from the MDC analysis. The shifts are measured from $T_P = 180$ K. (b) The ARPES intensity I_{FS} at the Fermi surface ($E=0$, $k=k_F^B$) is superposed on the spin susceptibility from Ref. 17.

Pretransitional fluctuations have been invoked[33] as a possible origin of the reduced spectral intensity at the Fermi surface in the normal state of Peierls systems. From the BCS relation $2\Delta_0 = 3.52 T_{MF}$ and from an analysis of the CDW dynamics,[25] one obtains $T_{MF} \sim 320$ K in $K_{0.3}MoO_3$. We have already pointed out[21] that fluctuations alone cannot explain the peculiar ARPES line shape of 1D Peierls systems. In a fluctuating pseudogap scenario, the spectral intensity is removed within an energy of the order of the Peierls gap below E_F, and the pseudogap evolves into a real gap below T_P. If fluctuations in the CDW state[34] are neglected, the spectrum merges with the mean-field spectrum in the $T=0$ limit. This is clearly not the case here, since the ARPES pseudogap scale is much larger than the Peierls gap, but fluctuations do have a measurable effect on the spectrum. This as illustrated in Fig. 7(b), where the ARPES intensity at the Fermi surface $I(k_F^B,0)$ is compared with the spin susceptibility from Ref. 17. The increase of χ_{spin} above T_P reflects the progressive filling-in of the pseudogap in the metallic phase. Within the experimental uncertainties $I(k_F^B,0)$ exhibits the same temperature dependence and therefore also reflects the temperature dependent pseudogap. This conclusion is not incompatible with the unusual line shape or with the opening of a Peierls gap below T_P [Fig. 7(a)]. As discussed below, the suppression of QP spectral weight is largely a consequence of interactions, but fluctuations above T_P further reduce the intensity at E_F. The QP DOS is therefore pseudogapped, and only when long-range coherence is established below T_P can a real gap develop.

C. Spectral line shape and the nature of the quasiparticles

The results of the previous sections establish the existence of band features and of characteristic fingerprints of the Peierls transition in $K_{0.3}MoO_3$. However, the dispersing peaks fail to cross the Fermi level in the metallic phase, and their minimum binding energies are unrelated to the typical energy scale of the material, the Peierls gap Δ_0. The spectral linewidth (~ 0.4 eV) is also unusually large. In a normal Fermi liquid, the width of a QP peak $\Delta E \sim \hbar/\tau$ is proportional to the inverse of the QP lifetime.[35] The conditions for the QP's to be well-defined excitations are $\Delta E < E$ and $\Delta \rightarrow 0$ at the Fermi surface (for $T \rightarrow 0$). Neither of these conditions is verified in $K_{0.3}MoO_3$ if we interpret the whole ARPES peak as a coherent excitation. However, a different interpretation is possible.

Strong interactions—or singular interactions in 1D—considerably modify the QP spectrum. They shift weight from the *coherent* QP peak to the *incohent* part of the spectrum over an energy range which depends on the interactions and which can be much larger than the intrinsic QP width. Strong, long-range electronic correlations in 1D can produce broad line shapes compatible with experimental ARPES spectra.[36] This indicates a promising approach to 1D systems with dominant electronic correlations, like some organic Bechgaard salts[37] or the Peierls system TTF-TCNQ,[11,38] where electronic correlations are relevant at least on the TTF chains.

There is no evidence of strong electronic correlations in standard Peierls systems like $K_{0.3}MoO_3$ or $(TaSe_4)_2I$, where the occurrence of a CDW ground state shows dominant electron-phonon (e-ph) interactions. An analysis of the CDW correlation length indicates a ''sizable'' e-ph coupling strength in $K_{0.3}MoO_3$.[25] Optics data also point to a large e-ph coupling parameter ($\lambda \sim 1.2$).[34] It is therefore tempting to interpret the broad ARPES line shapes of $K_{0.3}MoO_3$—and $(TaSe_4)_2I$—as the spectra of electrons strongly coupled to the lattice.

We have qualitatively discussed elsewhere[21] the expected spectral properties by analogy with the much simpler problem of a single electron coupled with a harmonic oscillator.[39] The spectrum exhibits a ''zero-phonon'' (or ''0-0'') peak and satellites at lower energy, under a common Poissonian envelope. The leading peak (adiabatic limit) corresponds to a transition between the ground states of the neutral and of the ionized system, and the satellites to transitions to vibrationally excited states. This *incoherent* part of the spectrum draws intensity from the ''0-0'' peak, which is progressively reduced as the coupling strength increases. The maximum of the spectrum occurs at an energy $E^* \sim \langle n \rangle \hbar\Omega$ below the leading peak, where $\langle n \rangle$ is the average number of quanta of vibration ''dressing'' the electron in the ground state and $\hbar\Omega$ is the frequency of the coupled mode. This simple model describes quite accurately the photoemission spectrum of a diatomic molecule like H_2,[40] and in that context the satellites are known as Frank-Condon satellites.

These simple considerations provide a qualitative guideline for the problem of a dense system of interacting electrons coupled to a lattice. Again we expect a progressive transfer of spectral weight from a ''zero-phonon'' peak to vibrational satellites with increasing coupling.[41] In a solid, of course, the interaction with a continuum of vibrational states plus various broadening mechanisms smear out the satellite structure, and only a (Gaussian) envelope will be observed. The weight of the leading peak reflects the progressively smaller overlap of the photohole with the real quasiparticle. For a sufficiently strong coupling the QP's can be described as small polarons, i.e., heavily dressed electrons which move coherently with the local lattice deformation. In this limit, the overlap between the QP and photohole wave functions is vanishingly small, and the coherent peak is exponentially

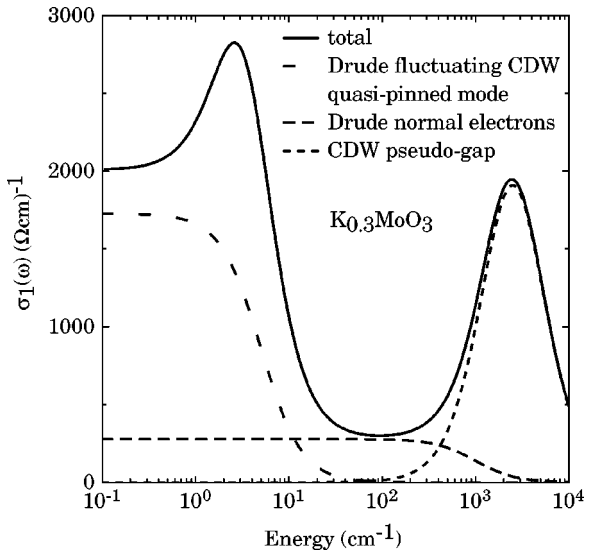

FIG. 8. Optical conductivity after the Lorentz-Drude model, based on the classical dispersion theory, reproducing the experimental data at $T=200$ K, along the chain direction (Ref. 18). The components of the calculation are shown separately, and the contributions from the polaronic QP's are highlighted as dashed surfaces.

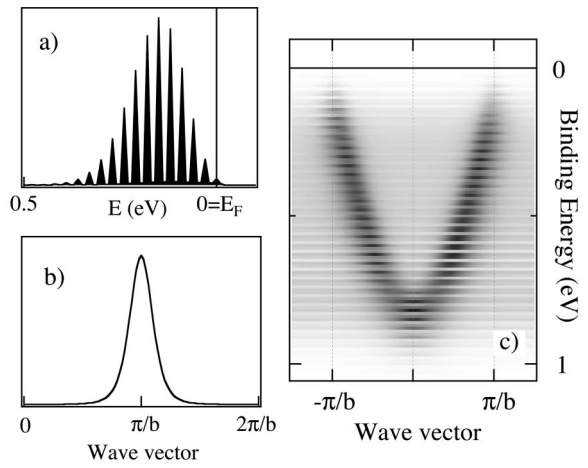

FIG. 9. (a) Calculated spectrum and (b) momentum distribution ($E=30$ meV) of a polaronic QP at the Fermi surface. The QP is dressed by $\langle n\rangle=5$ phonons with an energy of 30 meV, and the range of the e-ph interaction is 30 Å. (c) Momentum-dependent spectral weight distribution. The parameters of the underlying ''frozen lattice'' dispersion were chosen such as to reproduce the experimental ARPES dispersion.

reduced.[42] The essentially incoherent spectrum peaks at $E^* \sim\langle n\rangle\hbar\Omega^*$ below the QP energy, where Ω^* is an average frequency. Guassian line shapes—one for each valence band—fit well the spectra of $(TaSe_4)_2I$ and can also describe the blue bronze data.

From the energy separation between the QP energy—the Fermi energy at k_F in the metallic phase—and the maximum of the spectrum ($E^*=0.2$ eV) we can attempt a rough estimate of the structure of the phonon cloud. Neutron data show a large phonon density in the 10–50 meV range,[43] which yields $\langle n\rangle\sim 5$–10 phonons. A more accurate estimate would require an analysis of the coupling strengths. Namely, the relative importance of the low-frequency mode involved in the Kohn anomaly[25]—the precursor of the Peierls transition—and of the local, higher-frequency vibrations should be assessed. Even with these uncertainties, we conclude that heavily dressed electrons are compatible with the observed small QP weight in ARPES.

Optical data provide independent evidence for heavy QP's in $K_{0.3}MoO_3$. Figure 8 shows the real part of the optical conductivity $[\sigma(\omega)]$ for light polarized along the chain axis in the spectral range below 1 eV ($\sim 10^4$ cm^{-1}) at $T=200$ K, in the normal metallic phase.[18] Similar to our previous analysis on $(TaSe_4)_2I$,[21] we can identify several distinct components, which are well reproduced within the phenomenological Lorentz-Drude approach.[44] The main feature at $2\Delta=1000$ cm^{-1} (~ 120 meV) is associated with the Peierls pseudogap, which is already quite deep at this temperature. At low frequencies, the spectrum displays a rather complex behavior. Besides the peak ascribed to the quasi-pinned collective mode at about 3 cm^{-1}, there are two distinct zero-frequency modes. The first narrow Drude represents the collective contribution of the sliding CDW segments, while the second broad Drude reflects the response of the uncondensed quasiparticles.

The spectral weight of the QP component can be scaled with respect to the total spectral weight up to the threshold of the interband transition.[21] The integral[44] of $\sigma(\omega)$ leads to $\Omega_p^{tot}=25\,600$ cm^{-1}, while spectral weight arguments applied to the QP component yield $\Omega_p^{QP}=4100$ cm^{-1}. From the conductivity sum rule we find

$$(\Omega_p^{tot}/\Omega_p^{QP})^2=(n^{tot}/n)(m^*/m_e)=39. \quad (1)$$

Notice that m^* is the effective mass of the polaronic QP's, and should not be confused with the—much larger—mass of the fluctuating CDW segments. Using $n/n^{tot}\sim 0.7$ at 200 K derived from the spin susceptibility,[17] we obtain the polaron effective mass $m^*\sim 28m_e$. A comparison with the GGA band yields $m^*(200K)\sim 40m_{band}$.

In this polaronic scenario—and in a similar approach proposed in a different context in Refs. 45 and 46—the ARPES peaks of Figs. 1–3 do not represent the QP's, but the dispersing maxima of the incoherent spectrum. As discussed in Ref. 45 the suddenly created photohole ''sees'' a frozen lattice, where it could disperse with a velocity corresponding to the noninteracting band. Therefore ARPES reveals the unperturbed bandwidth, rather than the exponentially narrowed polaronic bands. However, the photohole is rapidly slowed down by the lattice deformation. The result is a ''blurred'' band, which can be interpreted as the superposition of narrow polaronic bands, where the spectral weight is concentrated along the frozen lattice dispersion. There is a clear distinction between bands, i.e., the k-dependent energy eigenvalues of the Hamiltonian, which are not directly observable, and the spectral weight which is a physical observable, measured in an ARPES experiment.[19]

This is well illustrated by a calculation along the lines of Ref. 47 for a QP dressed by $\langle n\rangle\sim 5$ phonons. As expected, the spectrum [Fig. 9(a)] is dominated by the *incoherent* satellites. The suppression of the leading QP peak and the shift

of spectral weight are controlled by the strength of the e-ph coupling. The momentum distribution is determined instead by the range r of the interaction. For a strictly local interaction, the spectral weight is uniformly distributed in k space. For a more realistic nonlocal interaction ($r=30$ Å) [Fig. 9(b)] the resulting MDC defines a coherence length ($l=1/\Delta k$) of the order of the size of the phonon cloud. The coherence length is larger than the unit cell, and the spectral weight is distributed along the frozen lattice band [Fig. 9(c)]. Notice that this simple calculation produces suggestive results, in agreement with our experiment, although we used it beyond its expected range of validity ($E^* <$ bandwidth).[47]

The MDC's of Fig. 5 indicate that the coherence lenght of the polaronic QP's is short ($l=1/\Delta k \sim 11$ Å when the experimental momentum resolution is taken into account), much shorter than the typical values (100–1000 Å) for normal metals. A pump-probe experiment[48] which directly measured the QP response in the time domain found a QP lifetime $\tau=0.5$ ps. From the relation $l=v_{QP}\tau$, where v_{QP} is the QP group velocity, we obtain $v_{QP}\sim 2\times 10^2$ ms^{-1}, which is about two orders of magnitude smaller than the average velocity for the B band. Therefore the underlying polaronic bands are much narrower than the GGA or ARPES bands, consistent with the strong coupling scenario.

We also notice that the QP coherence length is considerably shorter than the in-chain CDW coherence length at 200 K (~ 50 Å) (Ref. 25) and temperature independent. On the other hand, the QP coherence length is quite close to the CDW period ($\lambda_{CDW}\sim 9$ Å). Qualitatively, this is what one expects in a local picture of the CDW, which ignores the $2k_F$ instability and the nesting properties of the FS and where long-range order is achieved with condensation of local polaronic carriers. The coexistence of typical features of the weak-coupling Peierls scenario and of a strong-coupling approach shows that neither model of the transition is completely satisfactory. Apparently, after three decades of intensive investigation, a crucial issue of the physics of the blue bronze remains open.

V. CONCLUSIONS

We exploited high-resolution ARPES to study the band structure, the properties of the quasiparticle states, and the consequences (gap, periodicity) of the CDW instability in the typical 1D Peierls system $K_{0.3}MoO_3$. We find conduction bands with strong 1D character, in good agreement with previous ARPES work and with recent GGA band structure calculations. By examining their symmetry properties, we verified the assignment of the topmost bands to bonding and antibonding combinations of 1D bands on adjacent chains. These bands support a ''hidden'' Fermi surface with the nesting properties required by the Peierls model for the CDW transition. The temperature dependence of the spectrum at the estimated Fermi wave vectors exhibits clear signs of the transition. The spectra also exhibit signatures of a fluctuating CDW in the normal metallic phase.

The ARPES and optical spectral properties support strong electron-phonon interactions and the formation of small polarons with a large mass and a short (~ 10 Å) coherence length. The similarities between $K_{0.3}MoO_3$ and $(TaSe_4)_2I$ suggest that strong interactions and heavy polaronic QP's could be generic features of 1D Peierls systems, a hypothesis which calls for an experimental verification in other related materials. The coexistence of strong interactions and nonlocal aspects requires a further scrutiny of the origin of the CDW transition and a theory that extends the prevailing weak-coupling scenario. Finally, we notice that if the ARPES line shape of Peierls systems is dominated by the strong e-ph coupling, the expected spectral signatures of the Luttinger or Luther-Emery liquid—namely, spin-charge separation—would be confined at the leading edge of the broad spectrum. Their direct observation could be prohibitively difficult due to the vanishingly small intensity.

ACKNOWLEDGMENTS

We thank K. Kamaras for the generous loan of the crystals and E. Canadell for disclosing band structure calculations prior to publication. We also acknowledge many clarifying discussions with J. Voit and correspondence with J.-P. Pouget. This work was supported by the Swiss National Science Foundation under the NCCR program 'Materials with Novel Electronic Properties–MaNEP'. The SRC is supported by the NSF under Award No. DMR-0084402.

[1] G. Grüner, *Density Waves in Solids* (Addison-Wesley, Reading, MA, 1994).
[2] P. Y. Ledaron and S. Aubry, J. Phys. C **16**, 4827 (1983); J. L. Raimbault and S. Aubry, J. Phys.: Condens. Matter **7**, 8287 (1995); J. P. Lorenzo and S. Aubry, Physica D **113**, 276 (1998).
[3] F. D. M. Haldane, J. Phys. C **14**, 2585 (1981).
[4] J. Voit, Rep. Prog. Phys. **58**, 977 (1995).
[5] A. Luther and V. J. Emery, Phys. Rev. Lett. **33**, 589 (1974).
[6] J. Voit, J. Phys.: Condens. Matter **5**, 8305 (1993).
[7] V. Vescoli, L. Degiorgi, W. Henderson, G. Grüner, K. P. Starkey, and L. K. Montgomery, Science **281**, 1181 (1998).
[8] For a recent review see M. Grioni and J. Voit, in *Electron Spectroscopies Applied to Low-Dimensional Materials*, edited by H. P. Hughes and H. I. Starnberg (Kluwer, Dordrecht, 2000), p. 209.
[9] C. Kim, A. Y. Matsuura, Z.-X. Shen, N. Motoyama, H. Eisaki, S. Uchida, T. Tohyama, and S. Maekawa, Phys. Rev. Lett. **77**, 4054 (1996).
[10] J. D. Denlinger, G.-H. Gweon, J. W. Allen, C. G. Olson, J. Marcus, C. Schlenker, and L.-S. Hsu, Phys. Rev. Lett. **82**, 2540 (1999).
[11] R. Claessen, M. Sing, U. Schwingenschlögel, P. Blaha, M. Dressel, and C. S. Jacobsen, Phys. Rev. Lett. **88**, 096402 (2002).
[12] P. Segovia, D. Purdie, M. Hengsberger, and Y. Baer, Nature (Lon-

don) **402**, 504 (1999).
[13] J.-P. Pouget, in *Low Dimensional Electronic Properties of Molybdenum Bronzes and Oxides*, edited by C. Schlenker (Kluwer, Dordrecht, 1989), p. 87.
[14] P. A. Lee, T. M. Rice, and P. W. Anderson, Phys. Rev. Lett. **31**, 462 (1973).
[15] L. Bartosch and P. Kopietz, Phys. Rev. B **62**, 16 223 (2000).
[16] H. Monien, Phys. Rev. Lett. **87**, 126402 (2001).
[17] D. C. Johnston, Phys. Rev. Lett. **52**, 2049 (1984).
[18] A. Schwartz, M. Dressel, B. Alavi, A. Blank, S. Dubois, G. Grüner, B. P. Gorshunov, A. A. Volkov, G. V. Kozlov, S. Thieme, L. Degiorgi, and F. Levy, Phys. Rev. B **52**, 5643 (1995).
[19] J. Voit, L. Perfetti, F. Zwick, H. Berger, G. Margaritondo, G. Grüner, H. Höchst, and M. Grioni, Science **290**, 501 (2000).
[20] J. Schäfer, Eli Rotenberg, S. D. Kevan, P. Blaha, R. Claessen, and R. E. Thorne, Phys. Rev. Lett. **87**, 196403 (2001).
[21] L. Perfetti, H. Berger, A. Reginelli, L. Degiorgi, H. Höchst, J. Voit, G. Margaritondo, and M. Grioni, Phys. Rev. Lett. **87**, 216404 (2001).
[22] J. Dumas and C. Schlenker, Int. J. Mod. Phys. B **7**, 4045 (1993).
[23] M.-H. Whangbo and L. F. Schneemeyer, Inorg. Chem. **25**, 2424 (1986).
[24] E. Canadell and M.-H. Whangbo, Chem. Rev. **91**, 965 (1991).
[25] J. P. Pouget, S. Girault, A.H. Moudden, B. Hennion, C. Escribe-Filippini, and M. Sato, Phys. Scr. **T25**, 58 (1989).
[26] J.-L. Mozos, P. Ordejón, and E. Canadell, Phys. Rev. B **65**, 233105 (2002).
[27] B. Dardel, D. Malterre, M. Grioni, P. Weibel, Y. Baer, C. Schlenker, and Y. Petroff, Europhys. Lett. **19**, 525 (1992).
[28] G.-H. Gweon, J. D. Denlinger, J. W. Allen, R. Claessen, C. G. Olson, H. Höchst, J. Marcus, C. Schlenker, and L. F. Schneemeyer, J. Electron Spectrosc. Relat. Phenom. **117**, 481 (2001).
[29] G.-H. Gweon, J. W. Allen, R. Claessen, J. A. Clack, D. M. Poirier, P. J. Benning, C. G. Olson, W. P. Ellis, Y. X. Zhang, L. F. Schneemeyer, J. Marcus, and C. Schlenker, J. Phys.: Condens. Matter **8**, 9923 (1996).
[30] A. V. Fedorov, S. A. Brazovskii, V. N. Muthukumar, P. D. Johnson, J. Xue, L.-C. Duda, K. E. Smith, W. H. McCarrol, M. Greenblatt, and S. L. Hulbert, J. Phys.: Condens. Matter **12**, L191 (2000).
[31] M. Grioni, H. Berger, M. Garnier, F. Bommeli, L. Degiorgi, and C. Schlenker, Phys. Scr. **T66**, 172 (1996).
[32] C. Noguera, J. Phys. C **19**, 2161 (1985).
[33] N. Shannon and R. Joynt, J. Phys.: Condens. Matter **8**, 10493 (1996).
[34] L. Degiorgi, St. Thieme, B. Alavi, G. Grüner, R. H. McKenzie, K. Kim, and F. Levy, Phys. Rev. B **52**, 5603 (1995).
[35] L. Perfetti, C. Rojas, A. Reginelli, L. Gavioli, H. Berger, G. Margaritondo, M. Grioni, R. Gaal, L. Forro, and F. Rullier-Albenque, Phys. Rev. B **64**, 115102 (2001).
[36] P. Kopietz, V. Meden, and K. Schönhammer, Phys. Rev. Lett. **74**, 2997 (1995).
[37] F. Zwick, H. Berger, I. Vobornik, G. Margaritondo, L. Forro, C. Beeli, M. Onellion, G. Panaccione, A. Taleb-Ibrahimi, and M. Grioni, Phys. Rev. Lett. **81**, 1058 (1998).
[38] F. Zwick, D. Jérome, G. Margaritondo, and M. Onellion, Phys. Rev. Lett. **81**, 2974 (1998).
[39] G. D. Mahan, *Many-Particle Physics* (Plenum, New York, 1981).
[40] G. A. Sawatzky, Nature (London) **342**, 480 (1989).
[41] J. M. Robin, Phys. Rev. B **56**, 13 634 (1997).
[42] A. S. Mishchenko, N. V. Prokof'ev, A. Sakamoto, and B. V. Svistunov, Phys. Rev. B **62**, 6317 (2000).
[43] H. Requardt, R. Currat, P. Monceau, J. E. Lorenzo, A. J. Dianoux, J. C. Lasjaunias, and J. Marcus, J. Phys.: Condens. Matter **9**, 8639 (1997).
[44] F. Wooten, *Optical Properties of Solids* (Academic Press, New York, 1972).
[45] D. S. Dessau, T. Saitoh, C. H. Park, Z.-X. Shen, P. Vilella, N. Hamada, Y. Moritomo, and Y. Tokura, Phys. Rev. Lett. **81**, 192 (1998).
[46] V. Perebeinos and P. B. Allen, Phys. Rev. Lett. **85**, 5178 (2000).
[47] G. J. Kaye, Phys. Rev. B **57**, 8759 (1998).
[48] J. Demsar, K. Biljakovic, and D. Mihailovic, Phys. Rev. Lett. **83**, 800 (1999).